J Electr Eng Technol.2018; 13(6): 2319-2328
http://doi.org/10.5370/JEET.2018.13.6.2319

ISSN(Print) 1975-0102
ISSN(Online) 2093-7423

VPI-based Control Strategy for a Transformerless MMC-HVDC System Under Unbalanced Grid Conditions

Si-Hwan Kim*, June-Sung Kim*, Rae-Young Kim†, Jin-Tae Cho and Seok-Woong Kim****

Abstract – This paper introduces a control method for a transformerless MMC-HVDC system. The proposed method can effectively control the grid currents of the MMC-HVDC system under unbalanced grid conditions such as a single line-to-ground fault. The proposed method controls the currents of the positive sequence component and the negative sequence component without separating algorithms. Therefore, complicated calculations for extracting the positive sequence and the negative sequence component are not required. In addition, a control method to regulate a zero sequence component current under unbalanced grid conditions in the transformerless MMC-HVDC system is also proposed. The validity of the proposed method is verified through PSCAD/EMTDC simulation.

Keywords: Current control, High voltage direct current(HVDC) transmission system, Modular multi-level converter(MMC), Transformerless, Unbalanced grid, Vector proportional-integrator control.

1. Introduction

The modular multilevel converter (MMC) has been actively studied for application to motor drives, static synchronous compensators, and high-voltage direct current (HVDC) transmission systems due to its various advantages such as easy scalability of the voltage level, low harmonic content, and excellent fault reliability [1-3].

Several studies have been conducted to control MMC-HVDC system under grid fault conditions, especially single line-to-ground fault condition [4-14]. Reference [5] introduced two control methods for controlling MMC-HVDC system under unbalanced grid conditions. Reference [5] has been shown that the method to regulate the second harmonic component of the power introduced in [5] is not suitable for the MMC-HVDC system. Reference [6] revealed that the second harmonic ripple component is appeared in the DC voltage of the MMC-HVDC system under unbalanced grid conditions, and a method to regulate this ripple component is introduced. Methods to control the MMC-HVDC system based on the proportional-resonant (PR) controller in the stationary reference frame are introduced [7-11]. A method based on the model predictive control has also been introduced [12]. Reference [13] introduced a steady-state modeling for the MMC-HVDC system under unbalanced grid condition. Generic control method for the MMC-HVDC system under unbalanced grid conditions was studied in [14]. Most of the studies to control MMC-HVDC system have introduced in the presence of transformers.

In contrast, the MMC-HVDC system has advantages that it can control the zero sequence component unlike the conventional 2-level or 3-level converter based HVDC system. Therefore, the MMC-HVDC system can operate without a transformer to reduce the cost and space [5, 15-17]. Studies in the absence of a transformer were dealt with only few papers. Reference [5] introduced a method to control zero sequence component current through a PI controller. In [15], the control method of zero sequence component current based on the PR controller was introduced. The method using the quasi-PR controller is introduced in [16]. In [17], a method to compensate the negative sequence component and the zero sequence component of currents is described. These control strategies to control the MMC-HVDC system without a transformer are based on the method of extracting or calculating the negative sequence component to regulate the negative sequence component under unbalanced grid conditions. These methods have a disadvantage in that a complicated operation is required to separate the positive sequence and negative sequence component. Also, since the zero sequence component is an AC component at the same frequency as the grid voltage frequency, it is difficult to control the steady-state error to 0 in the method using the PI controller. The control method using the PR controller or the quasi-PR controller has a disadvantage in that the selection of the control gain value is complicated, although the steady state error can be improved due to a large gain value in the resonance frequency.

In order to recover disadvantages, this paper proposes a control scheme based on the vector-PI (VPI) controller in

† Corresponding Author: Dept. of Electrical and Biomedical Engineering, Hanyang University, Korea. (rykim@hanyang.ac.kr)
* Dept. of Electrical Engineering, Hanyang University, Korea. ({rlatis, uramee305}@hanyang.ac.kr)
** Korea Electric Power Research Institute(KEPRI), Korea Electric Power, Corporation(KEPCO), Daejeon, Korea. ({jintae.cho, sw.kim}@kepco.co.kr)
Received: October 11, 2017; Accepted: July 6, 2018

the synchronous reference frame for the transformerless MMC-HVDC system. The proposed scheme does not require a complicated operation for extracting positive sequence and negative sequence component. Both positive sequence and negative sequence currents are controlled both in positive synchronous reference frame. Thus, the computational burden for current control can be reduced. Also, proposed control scheme can regulate the zero sequence current to zero under unbalanced grid conditions through a large control gain in the resonance frequency. The all current controller gain is selected based on the pole-zero cancellation technique, thus, easy to select.

This paper is composed as follows. Section 2 shows the basic structure and mathematical model of the MMC-HVDC system. Section 3 introduces the proposed control scheme. Section 4 verifies the effectiveness of the proposed method through simulation results. Section 5 concludes.

2. MMC-HVDC system

2.1 Basic configuration

Fig. 1 shows a configuration of the transformerless MMC-HVDC system. Each converter station is connected to a point of common coupling (PCC) of AC grid through a system reactor L_g and connected through a back-to-back structure.

Fig. 2 shows a basic configuration of MMC. The three

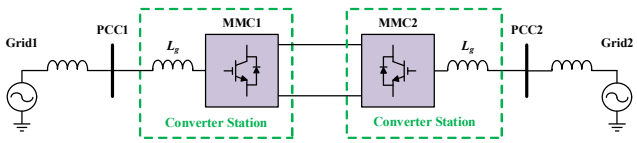

Fig. 1. Configuration of the transformerless MMC-HVDC system

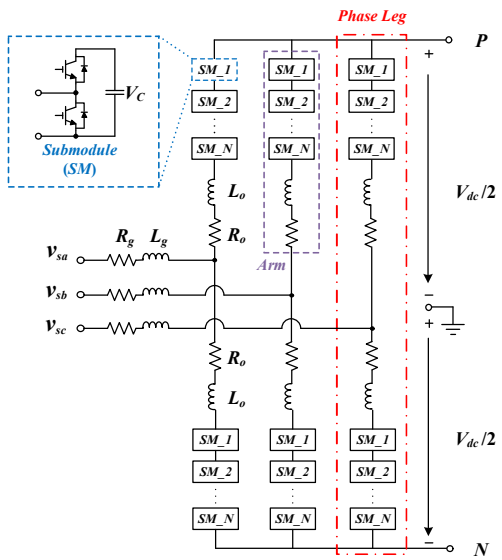

Fig. 2. Basic configuration of MMC

legs in MMC are connected to PCC through a system reactor L_g, and each leg consists of two arms. The arm consists of N sub-modules (SMs) and arm reactor L_o, and each sub-module (SM) has a same half-bridge structure. The number of SMs per arm is can be calculated from the rated DC link voltage V_{dc} and rated SM capacitor voltage V_c. The sum of the rated capacitor voltages of all SMs should be equal the rated DC link voltage. In Fig. 2, v_{sj} is a PCC voltage, R_g is an equivalent resistance of L_g, R_o is an equivalent resistance of L_o, and j represents the a, b, and c phase.

2.2 Mathematical model

The single phase equivalent circuit of MMC for mathematical modeling is depicted in Fig. 3. Applying the Kirchhoff's voltage law to the upper and lower arms to control the grid current, (1) and (2) are obtained.

$$v_{sj} = \frac{V_{dc}}{2} - V_{pj} - L_o \frac{di_{pj}}{dt} - R_o i_{pj} - L_g \frac{di_{gj}}{dt} - R_g i_{gj} \quad (1)$$

$$v_{sj} = -\frac{V_{dc}}{2} + V_{nj} + L_o \frac{di_{nj}}{dt} + R_o i_{nj} - L_g \frac{di_{gj}}{dt} - R_g i_{gj} \quad (2)$$

where, i_{gj} is the grid current, V_{pj} and V_{nj} are the upper and lower arm voltages, i_{pj} and i_{nj} are the upper and lower arm currents, respectively.

The sum of (1) and (2) can be expressed as follow.

$$v_{sj} = v_{oj} - L_{eq} \frac{di_{gj}}{dt} - R_{eq} i_{gj} \quad (3)$$

where, the control variable v_{oj}, the equivalent inductance L_{eq}, and the equivalent resistance R_{eq} are as follows.

$$\begin{cases} v_{oj} = \left(V_{nj} - V_{pj}\right)/2 \\ L_{eq} = L_g + L_0/2 \\ R_{eq} = R_g + R_o/2 \end{cases} \quad (4)$$

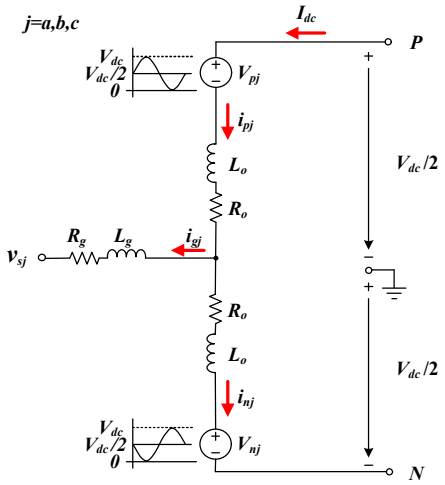

Fig. 3. Single-phase equivalence circuit of MMC

From (3), it can be seen that i_{gj} can be controlled directly via v_{oj}.

3. The Proposed Control Method

In a normal grid condition, the grid currents contain the positive sequence component only. However, if unbalanced grid condition such as a single line-to-ground fault occurs, the positive sequence component, the negative sequence component, and the zero sequence component exist together in the grid currents as shown in (5). If (5) is transformed into the positive sequence synchronous reference frame using the transformation matrix, it can be expressed by (6).

$$i_{abc}=\begin{bmatrix} i_a \\ i_b \\ i_c \end{bmatrix} = \begin{bmatrix} I^+\cos(\theta+\varphi^+)+I^-\cos(\theta+\varphi^-)+I^0\cos(\theta+\varphi^0) \\ I^+\cos\left(\theta-\frac{2}{3}\pi+\varphi^+\right)+I^-\cos\left(\theta+\frac{2}{3}\pi+\varphi^-\right)+I^0\cos(\theta+\varphi^0) \\ I^+\cos\left(\theta+\frac{2}{3}\pi+\varphi^+\right)+I^-\cos\left(\theta-\frac{2}{3}\pi+\varphi^-\right)+I^0\cos(\theta+\varphi^0) \end{bmatrix} \tag{5}$$

$$i_{dq0}=T(\theta)i_{abc}=\begin{bmatrix} I^+\cos(\varphi^+)+I^-\cos(2\theta+\varphi^-) \\ I^+\sin(\varphi^+)-I^-\sin(2\theta+\varphi^-) \\ I^0\cos(\theta+\varphi^0) \end{bmatrix} \tag{6}$$

where, $\theta=\omega_g t$ and ω_g is angular frequency of the grid. I^+, I^-, and I^0 are peak values of the positive sequence, negative sequence, and zero sequence components, respectively, and φ^+, φ^-, and φ^0 are the phase angles of the positive sequence, negative sequence, and zero sequence components. In (6), the negative sequence component is expressed as an AC component having a frequency twice the grid frequency in the dq-axis. The zero sequence component is an AC component having the same frequency as the grid frequency.

The transformation matrix $T(\theta)$ is as follow.

$$T(\theta)=\frac{2}{3}\begin{bmatrix} \cos(\theta) & \cos\left(\theta-\frac{2}{3}\pi\right) & \cos\left(\theta+\frac{2}{3}\pi\right) \\ -\sin(\theta) & -\sin\left(\theta-\frac{2}{3}\pi\right) & -\sin\left(\theta+\frac{2}{3}\pi\right) \\ \frac{1}{2} & \frac{1}{2} & \frac{1}{2} \end{bmatrix} \tag{7}$$

The block diagram of the proposed controller is shown in Fig. 4. In the positive sequence synchronous reference frame, the positive sequence component is represented as a DC component in the d-axis and q-axis, so is controlled through the PI controller denoted $G_{PI,+}(s)$. Since the negative sequence component is represented as second harmonic on the positive sequence synchronous reference

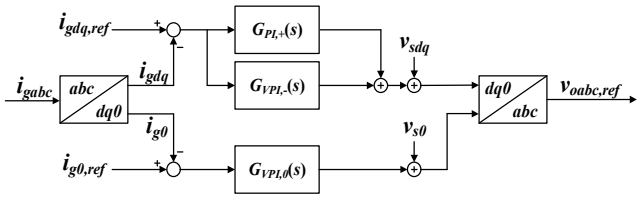

Fig. 4. Proposed current control scheme

frame, it is controlled through the VPI controller denoted $G_{VPI,-}(s)$ and the resonance frequency of the VPI controller is set to twice the grid frequency. The zero sequence component is also controlled by the VPI controller denoted $G_{VPI,0}(s)$, and the resonance frequency has the same frequency as the grid frequency. The transfer function of the PI controller and the VPI controller applied to the control scheme is expressed by (8) and (9) respectively [18-20].

$$G_{PI}(s)=K_p+\frac{K_i}{s} \tag{8}$$

$$G_{VPI}(s)=2\frac{\left(K_{pv}s^2+K_{iv}s\right)}{s^2+\omega_0^2} \tag{9}$$

where k_p is the proportional gain of the PI controller, k_i is the integral gain of the PI controller, k_{pr} is the proportional gain of the VPI controller, k_{ir} is the resonant gain of the VPI controller, and ω_0 is the angular frequency of the resonant point.

The system transfer function (10) is obtained from (3).

$$G_p(s)=\frac{1}{sL_{eq}+R_{eq}} \tag{10}$$

3.1 The positive sequence and negative sequence current controllers

In the proposed control scheme, the integral gains of the controllers should be selected as $K_i=K_pR_{eq}/L_{eq}$ and $K_{iv}=K_{pv}R_{eq}/L_{eq}$ to apply the pole-zero cancellation technique. Then, the response characteristic of the system is determined by K_p and K_{pv}.

A frequency response of the conventional PI controller based method and the proposed PI-VPI controller based method in the positive sequence synchronous reference frame is shown in Fig. 5 and Fig. 6. Fig. 5 shows open-loop transfer function of PI controller based system and PI-VPI controller based system. In Fig. 5, both control scheme have large DC gain. However, it can be seen that the gain of the PI-based control scheme is very low in the frequency range of twice the grid frequency in Fig. 5(a). In contrast, the gain in Fig. 5(b) is very large at the corresponding frequency due to the VPI controller.

Fig. 6 shows closed-loop transfer function of PI controller based system and PI-VPI controller based system. As shown in Fig. 6(a), the positive sequence component can be

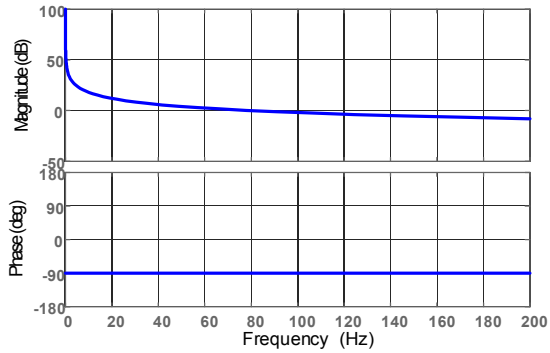

(a)

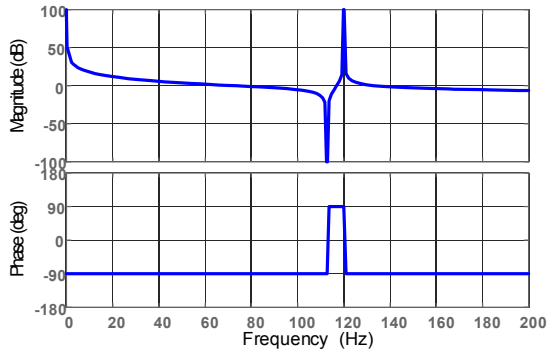

(b)

Fig. 5. The bode plot of open-loop transfer function (a) PI controller (b) PI-VPI controller

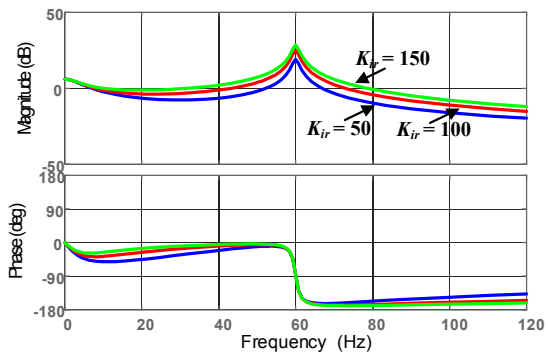

(a)

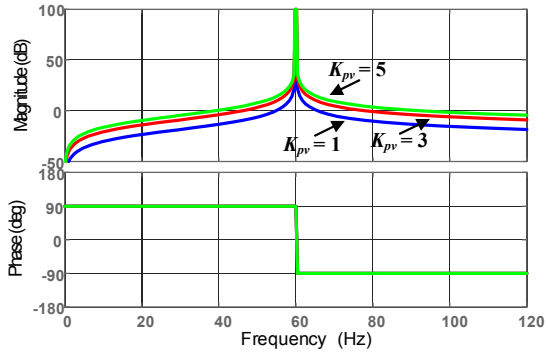

(b)

Fig. 7. The bode plot of open-loop transfer function (a) quasi-PR controller (b) VPI controller

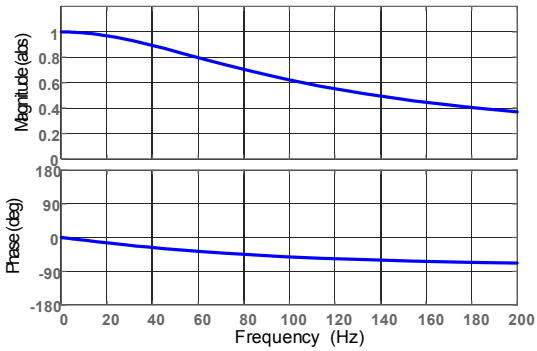

(a)

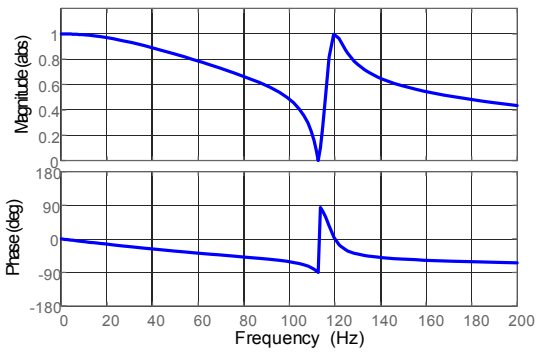

(b)

Fig. 6. The bode plot of closed-loop transfer function (a) PI controller (b) PI-VPI controller

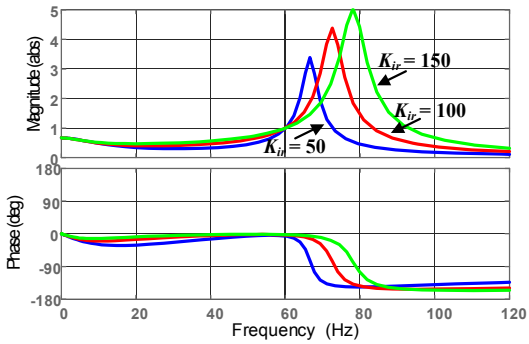

(a)

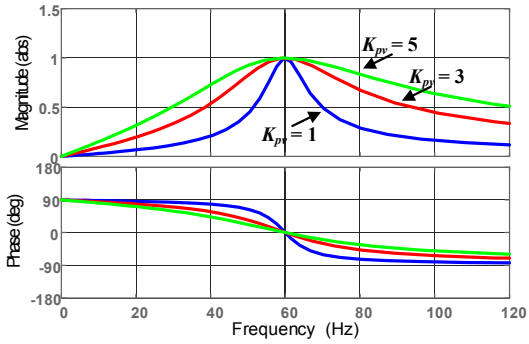

(b)

Fig. 8. The bode plot of closed-loop transfer function (a) quasi-PR controller (b) VPI controller

regulated well in the steady-state. However, the negative sequence component cannot be regulated because the gain at 120Hz is small and the phase delay is occurred. On the other hand, in Fig. 6(b), PI-VPI controller based system has no phase delay and the gain is 1 at 120Hz. Thus, this system can not only regulate the positive sequence component but also suppress the negative sequence component.

3.2 Zero sequence current controller

Fig. 7 and Fig. 8 show the frequency response of the quasi-PR controller based method and the VPI controller based method to analysis the characteristics of the controller. The transfer function of the quasi-PR controller is as follow [16].

$$G_{PR}(s) = K_{pr} + \frac{2K_{ir}\omega_c s}{s^2 + 2\omega_c s + \omega_0^2} \tag{11}$$

As shown in Fig. 7, both controllers provide a large gain at the grid frequency of 60 Hz.

In Fig. 8, both methods show a gain of 1 and no phase delay at the grid frequency. However, as shown in Fig. 8 (a), the quasi-PR controller based system shows an unwanted gain in the vicinity of grid frequency. Thus, if the controller gain is not properly selected, the system may become unstable. In contrast, Fig. 8(b) shows that in the system based on the VPI controller undesired gain does not appear regardless of the controller gain value.

3.3 VPI controller design for negative and zero sequence current

In this section, the design method of the proposed control scheme is discussed. Since a design method of the PI controller is well known [21], a design method of the VPI controller is described.

In the range of twice grid frequency, the closed-loop transfer function of the positive and negative sequence components controller can be expressed as follows.

$$G_{cl,-}(s) \approx \frac{G_{VPI,-}(s)G_P(s)}{1+G_{VPI,-}(s)G_P(s)} = \frac{2\frac{K_{pv,-}}{L_{eq}}s}{s^2 + 2\frac{K_{pv,-}}{L_{eq}}s + (2\omega_g)^2} \tag{12}$$

Similarly, the closed-loop transfer function of the zero sequence component controller in the range of grid frequency can be expressed as follows.

$$G_{cl,0}(s) = \frac{G_{VPI,0}(s)G_P(s)}{1+G_{VPI,0}(s)G_P(s)} = \frac{2\frac{K_{pv,0}}{L_{eq}}s}{s^2 + 2\frac{K_{pv,0}}{L_{eq}}s + \omega_g^2} \tag{13}$$

In (12) and (13), it can be seen that the closed-loop transfer function of the negative sequence current controller and the zero sequence current controller are in the form of a second-order bandpass filter as shown in (14).

$$G_{BPF}(s) = \frac{2\omega_{cc}s}{s^2 + 2\omega_{cc}s + \omega_{0,BPF}{}^2} \tag{14}$$

where ω_{cc} is the bandwidth of the bandpass filter, $\omega_{0,BPF}$ is the center frequency of the bandpass filter.

Comparing (12) and (13) to (14), it can be seen that the proportional gain of the VPI controller can be obtained from the desired bandwidth.

$$K_{pv,-} = \omega_{cc,-}L_{eq} \tag{15}$$

$$K_{pv,0} = \omega_{cc,0}L_{eq} \tag{16}$$

where, $\omega_{cc,-}$ is a bandwidth of the negative sequence current controller and $\omega_{cc,0}$ is a bandwidth of the zero sequence current controller.

Assuming that f_{min} and f_{max} are the minimum and maximum bandwidths, respectively, in the VPI controller, the range of K_{pv} can be obtained from (17) as shown in (18).

$$2\pi f_{\min} \le \omega_{cc} \le 2\pi f_{\max} \tag{17}$$

$$2\pi f_{\min}L_{eq} \le K_{pv} \le 2\pi f_{\max}L_{eq} \tag{18}$$

f_{min} can be set as a maximum variation of the grid frequency so as to be robust against the variation of the grid frequency. The larger f_{max}, the faster the response, but the range of 20Hz-60Hz can be selected considering the performance of the PI based controller for the positive sequence currents. In this paper, f_{min} and f_{max} are selected as 1Hz and 20Hz, respectively.

Table 1. The parameters of the simulation system

Parameters	Value
Active power	30 MW
Reactive power	0 Mvar
AC grid voltage (Line-to-line, rms)	42 kV
AC grid frequency	60 Hz
DC link voltage	80 kV
Grid impedance	1.13 Ω
Grid impedance angle	89 °
Grid reactor L_g	20 mH
Equivalent grid resistor R_g	0.5 Ω
Arm reactor L_o	20 mH
Equivalent arm resistor R_o	0.5 Ω
SM capacitance C_{SM}	6000 μF
Number of SMs per arm	80
Pos. seq. current controller P-gain, $K_{p,+}$	18.8
Pos. seq. current controller I-gain, $K_{I,+}$	471.2
Neg. seq. current controller P-gain, $K_{pv,-}$	2.8
Neg. seq. current controller R-gain, $K_{iv,-}$	70.7
Zero seq. current controller P-gain, $K_{pv,0}$	2.8
Zero seq. current controller R-gain, $K_{iv,0}$	70.7

4. Simulation Results

To verify the effectiveness of the proposed method, a simulation were performed through the PSCAD/EMTDC. The simulation parameters are shown in Table 1 and the configuration of the simulation model is same as Fig. 1. The PSCAD/EMTDC solution time step was set as 100us. In simulation studies, MMC-1 controls DC-link voltage and reactive power, and MMC-2 controls active power and reactive power. First, to verify the performance under normal balanced grid condition, the active power is stepped up from 15MW to 25MW at t = 0.5s and the reactive power is stepped up from 0Mvar to 5Mvar at t = 0.7s. Then, in order to verify the effectiveness under unbalanced grid conditions, single line-to-ground fault is occurred in phase-C of PCC-2 from t = 0.5 s to t = 0.8 s. According to [5], since the method of controlling the power of the second harmonic to 0 under unbalanced grid conditions is not suitable for the MMC, the method of maintaining the 3-phase balanced current under unbalanced grid conditions is applied.

Fig. 9 shows the simulation results of the conventional PI based control method under normal balanced grid condition. Fig. 9(a) shows the PCC voltages on the MMC-2 side and Fig. 9(b) shows the DC-link voltage of the MMC-HVDC system. Under normal balanced grid conditions, the DC-link voltage is well controlled at rated voltage. In Fig. 9(c), the active power is stepped up at t = 0.5s and the reactive power is stepped up at t = 0.7s. It can be shown that both active power and reactive power track

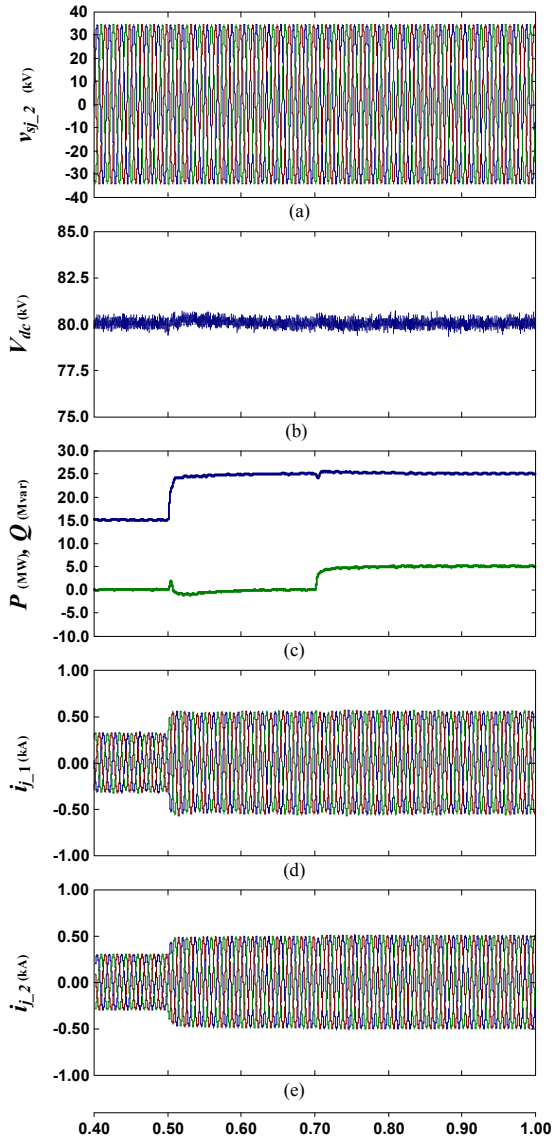

Fig. 9. Simulation waveforms of the conventional method: (a) PCC2 voltages; (b) DC-link voltage; (c) MMC2 active and reactive power; (d) MMC1 grid currents; (e) MMC2 grid currents

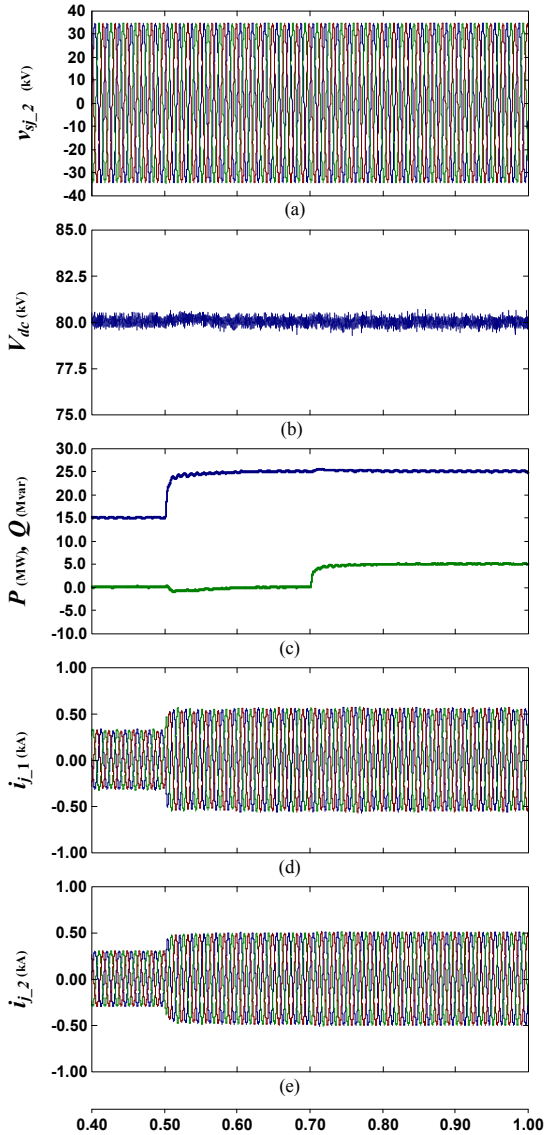

Fig. 10. Simulation waveforms of the proposed method: (a) PCC2 voltages; (b) DC-link voltage; (c) MMC2 active and reactive power; (d) MMC1 grid currents; (e) MMC2 grid currents

the reference value well. Fig. 9(d) and (e) show the grid current waveforms of MMC-1 and MMC-2. Since a time constant of the PI controller is set to about 2ms, it can be seen that the current reaches the steady state after about 10ms after the reference value is changed. Also, it can be seen that the currents of MMC-1 and MMC-2 are well

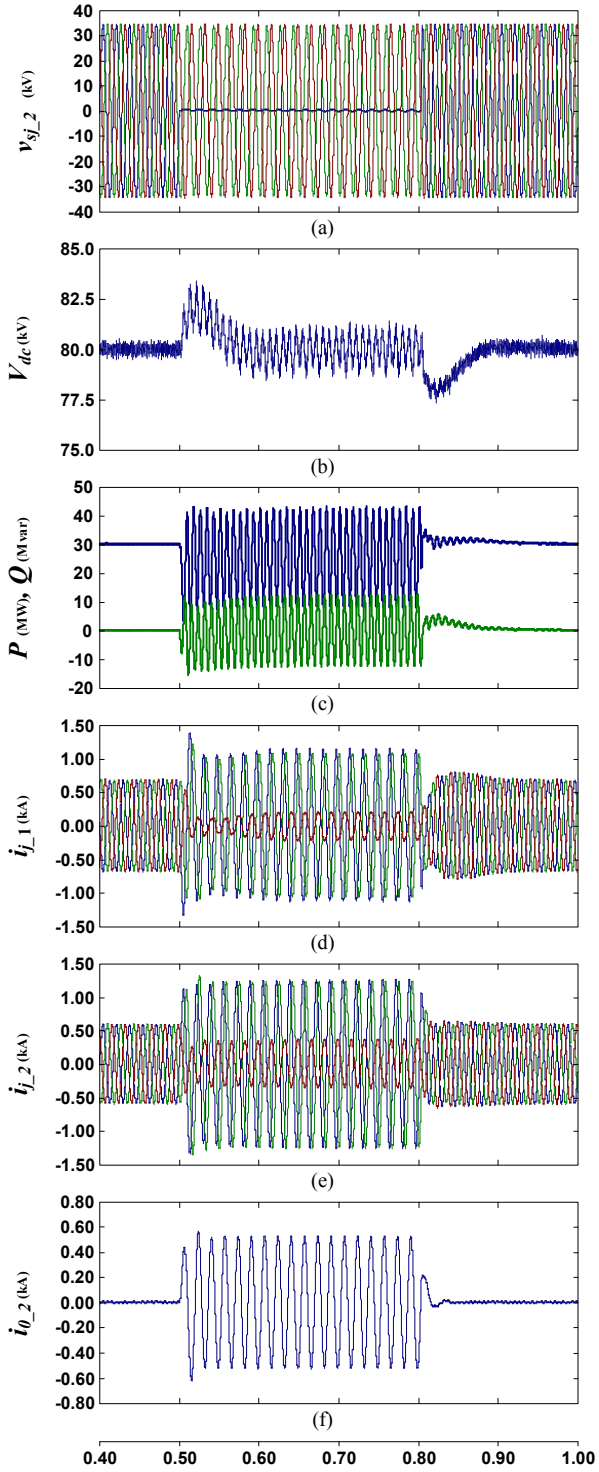

Fig. 11. Simulation waveforms of the conventional method: (a) PCC2 voltages; (b) DC-link voltage; (c) MMC2 active and reactive power; (d) MMC1 grid currents; (e) MMC2 grid currents; (f) zero sequence current of PCC2

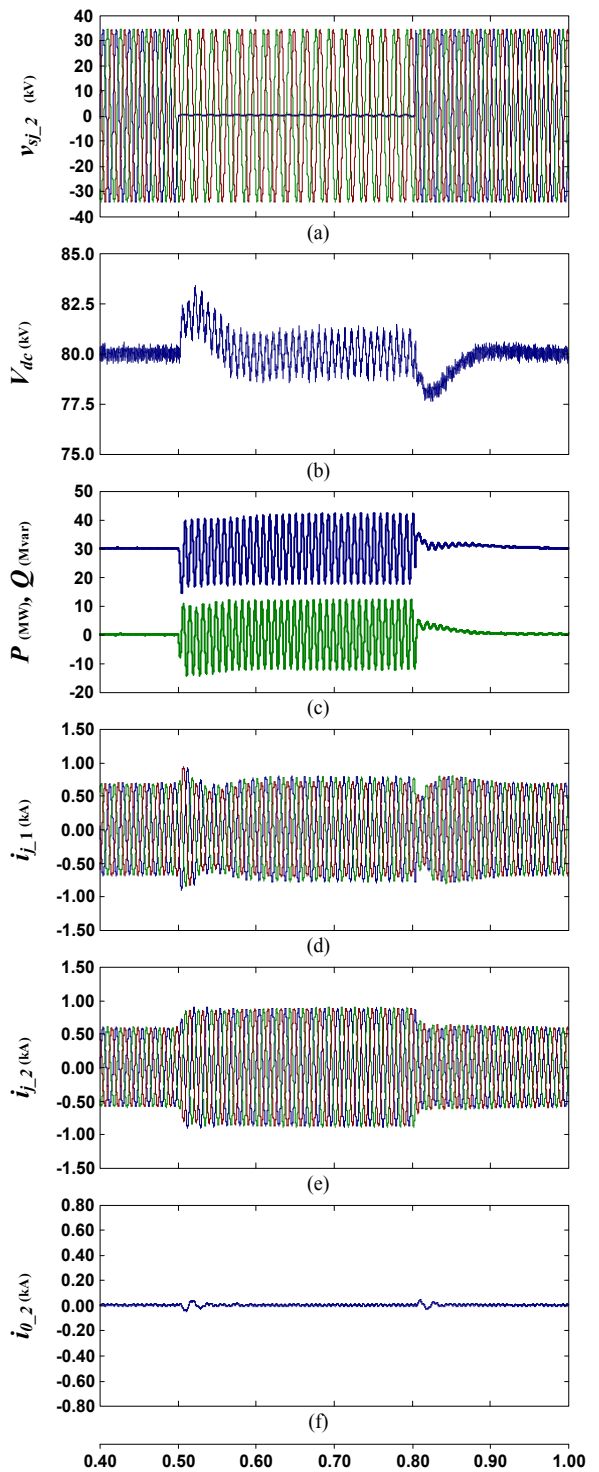

Fig. 12. Simulation waveforms of the proposed control method: (a) PCC2 voltages; (b) DC-link voltage; (c) MMC2 active and reactive power (d) MMC1 grid currents; (e) MMC2 grid currents; (f) zero sequence current of PCC2

regulated under normal balanced grid condition.

Fig. 10 shows the simulation results of the proposed current control method. Under normal balanced grid condition, the currents have only the positive sequence component. Thus, the system response characteristic is determined by the PI controller. Fig. 9 and Fig. 10 show that the response characteristics are similar because the PI controller gain is the same as the PI controller gain of the conventional method. Thus, it can be seen that the PI controller is hardly affected by the VPI controller.

Fig. 11 shows the simulation results of the conventional PI based control method with the positive sequence and negative sequence currents are controlled but the zero sequence current is not controlled. Fig. 11(a) shows the PCC voltages on the MMC-2 side and Fig. 11(b) shows the DC-link voltage of the MMC-HVDC system. In the normal balanced grid conditions, the DC-link voltage is well controlled at rated voltage. During a fault, it can be seen that there is a second harmonic ripple component in the DC-link voltage. In Fig. 11(c), the active and reactive power on the MMC-2 side are maintained at the rated power under normal grid condition. However, if the fault occurs in the grid, it can be shown that both active and reactive power contain the second harmonic component. Fig. 11(d) and (e) show the grid current waveforms of MMC-1 and MMC-2. In Fig. 11(d) and (e), during the fault the currents are not balanced because of the zero sequence current as shown in Fig. 11(f). Thus, in the absence of a transformer, the zero sequence component must be properly controlled.

Fig. 12 shows the simulation results of the proposed current control method. The second ripple component of the DC-link voltage in the fault condition is shown in Fig. 12(b), which showed similar to that found in Fig. 11(b). Comparing Fig. 11(c) and Fig. 12(c), it can be seen that the magnitude of the pulsating component of active power is reduced in the fault condition because the zero sequence current is controlled. The power due to the zero sequence component appears only in the active power, which generates pulsation to the active power. Therefore, if the zero sequence current is regulated to 0, the active power by the zero sequence component is not generated. Therefore, the magnitude of the pulsating component of the active power is reduced under unbalanced grid conditions as shown in Fig. 12(c). Fig. 12(d) and (e) show the grid currents waveforms of MMC-1 and MMC-2. Unlike Fig. 11(d) and (e), the currents are well balanced even when unbalance occurs in the grid. In Fig. 12(f), it can be seen that the zero sequence current is well regulated to 0. Thus, the proposed method effectively controls the grid currents of the MMC-HVDC system without transformer under unbalanced grid conditions.

5. Conclusion

In this paper, control scheme of the transformerless MMC-HVDC system is proposed. The mathematical model of the MMC-HVDC system is derived for the controller design. Under unbalanced grid conditions, the proposed control scheme controls the negative sequence component represented of second harmonic in the positive sequence synchronous reference frame. Also, since the zero sequence component appears as an alternating current at the same frequency as the grid frequency, a method for controlling the zero sequence component is introduced. The proposed method does not require a complicated algorithm for separating the negative sequence component, which can reduce the computational complexity and simplify the control structure. Also, it is easy to select the controller gain through the pole-zero cancellation technique. The proposed method can reduce cost and space by transformer by effectively controlling the grid currents. The effectiveness of the proposed method is verified through PSCAD/EMTDC.

Acknowledgements

This work was supported by the Korea Electric Power Research Institute through the project entitled by "Demonstration Study for Low Voltage Direct Current Distribution Network in an Island" under Grant R15DA12.

References

[1] Marcelo A. Perez, Steffen Bernet, Jose Rodriguez, Samir Kouro, and Ricardo Lizana, "Circuit Topologies, Modeling, Control Schemes, and Applications of Modular Multilevel Converters," *IEEE Trans. Power Electronics*, vol. 30, pp. 4-17, Jan. 2015.

[2] Alireza Nami, Jiaqi Liang, Frans Dijkhuizen, and Georgios D. Demetriades, "Modular Multilevel Converters for HVDC Applications: Review on Converter Cells and Functionalities," *IEEE Trans. Power Electronics*, vol. 30, pp. 18-36, Jan. 2015.

[3] Suman Debnath, Jiangchao Qin, Behrooz Bahrani, Maryam Saeedifard, and Peter Barbosa, "Operation, Control, and Applications of the Modular Multilevel Converter: A Review," *IEEE Trans. Power Electronics*, vol. 30, pp. 37-53, Jan. 2015.

[4] Maryam Saeedifard and Reza Iravani, "Dynamic Performance of a Modular Multilevel Back-to-Back HVDC System," *IEEE Trans. Power Delivery*, vol. 25, pp. 2903-2912, Oct. 2010.

[5] Minyuan Guan and Zheng Xu, "Modeling and Control of a Modular Multilevel Converter-Based HVDC System Under Unbalanced Grid Conditions," *IEEE Trans. Power Electronics*, vol. 27, pp. 4858-4867, Dec. 2012.

[6] Qingrui Tu, Zheng Xu, Yong Chang, and Li Guan, "Suppressing DC Voltage Ripples of MMC-HVDC

Under Unbalanced Grid Conditions," *IEEE Trans. Power Delivery*, vol. 27, pp. 1332-1338, July 2012.
[7] Zhou Yuebin, Jiang Daozhuo, Guo Jie, Hu Pengfei, and Lin Zhiyong, "Control of Modular Multilevel Converter Based on Stationary Frame under Unbalanced AC System," *in Proceedings of ICDMA Conference*, GuiLin, China, July 2012.
[8] Hu Pengfei, Jiang Daozhuo, Zhou Yuebin, Guo Jie, and Lin Zhiyong, "Study of the Proportional Resonant Control Based Modular Multilevel Converter," *in Proceedings of ICDMA Conference*, GuiLin, China, July 2012.
[9] Zhou Yuebin, Jiang Daozhuo, Jie Guo, Pengfei Hu, and Yiqiao Liang, "Analysis and Control of Modular Multilevel Converters Under Unbalanced Conditions," *IEEE Trans. Power Delivery*, vol. 28, pp. 1986-1995, Oct. 2013.
[10] Ngoc-Thinh Quach, Ji-Han Ko, Dong-Wan Kim, and Eel-Hwan Kim, "An Application of Proportional-Resonant Controller in MMC-HVDC System under Unbalanced Voltage Conditions," *Journal of Electrical Engineering & Technology*, vol. 9, pp. 1746-1752, Sep. 2014.
[11] Shaohua Li, Xiuli Wang, Zhiqing Yao, Tai Li, and Zhong Peng, "Circulating Current Suppressing Strategy for MMC-HVDC Based on Nonideal Proportional Resonant Controllers Under Unbalanced Grid Conditions," *IEEE Trans. Power Electronics*, vol. 30, pp. 387-397, Jan. 2015.
[12] Ji-Woo Moon, Jin-Su Gwon, Jung-Woo Park, Dae-Wook Kang, and Jang-Mok Kim, "Model Predictive Control With a Reduced Number of Considered States in a Modular Multilevel Converter for HVDC System," *IEEE Trans. Power Delivery*, vol. 30, pp. 608-617, Apr. 2015.
[13] Xiaojie Shi, Zhiqiang Wang, Bo Liu, Remus Yalong Li, Leon M. Tolbert, and Fred Wang, "Steady-State Modeling of Modular Multilevel Converter under Unbalanced Grid Conditions," *IEEE Trans. Power Electronics*, vol. 32, pp. 7306-7324, Sep. 2017.
[14] Anton Stepanov, Hani Saad, Jean Mahseredjian, and Aurélien Wataré, "Overview of Generic HVDC-MMC Control under Unbalanced Grid Conditions," *in Proceedings of IPST 2017 Conference, Seoul, Korea,* Jun. 2017.
[15] Artjoms Timofejevs, Daniel Gamboa, Marco Liserre, Remus Teodorescu, and Sanjay K. Chaudhary, "Control of transformerless MMC-HVDC during asymmetric grid faults," *in Proceedings of IECON 2013 Conference, Vienna, Austria,* Nov. 2013.
[16] Xiaojie Shi, Zhiqiang Wang, Bo Liu, Yiqi Liu, Leon M. Tolbert, and Fred Wang, "Characteristic Investigation and Control of a Modular Multilevel Converter-Based HVDC System Under Single-Line-to-Ground Fault Conditions," *IEEE Trans. Power Electronics*, vol. 30, pp. 408-421, Jan. 2015.
[17] Ghazal Falahi and Alex Huang, "Control of modular multilevel converter based HVDC systems during asymmetrical grid faults," *in Proceedings of IECON* 2014 *Conference, Dallas, TX, USA,* Nov., 2014.
[18] Cristian Lascu, Lucian Asiminoaei, Ion Boldea, and Frede Blaabjerg, "High performance current controller for selective harmonic compensation in active power filters," *IEEE Trans. Power Electronics*, vol. 22, pp. 1826-1835, Sep. 2007.
[19] Cristian Lascu, Lucian Asiminoaei, Ion Boldea, and Frede Blaabjerg, "Frequency Response Analysis of Current Controllers for Selective Harmonic Compensation in Active Power Filters," *IEEE Trans. Industrial Electronics*, vol. 56, pp. 337-347, Feb. 2009.
[20] Quoc-Nam Trinh and Hong-Hee Lee, "An Advanced Current Control Strategy for Three-Phase Shunt Active Power Filters," *IEEE Trans. Industrial Electronics*, vol. 60, pp. 5400-5410, Dec. 2013.
[21] Amirnaser Yazdani, Reza Iravani, "Dynamic model and control of the NPC-based Back-to-Back HVDC system," *IEEE Trans. Power Delivery*, vol. 21, pp. 414-424, Jan. 2006.

Si-Hwan Kim He received the B.S degree in Electrical Engineering from Hanyang University, Seoul, Korea, in 2013, where he is currently working toward the direct Ph.D. degree in the Department of Electrical Engineering, Hanyang University, Seoul, Korea. His current research interests include power transmission and distribution system and grid-connected power converter.

June-Sung Kim He received M.S degree in Electrical Engineering from Hanyang university, Seoul, Korea, in 2003, where he is currently working toward the Ph.D. degree in the Department of Electrical Engineering, Hanyang University, Seoul, Korea. His current research interests are MMC-HVDC and STATCOM.

Rae-Young Kim He received the B.S. and M.S. degrees from Hanyang University, Seoul, Korea, in 1997 and 1999, respectively, and the Ph.D. degree from Virginia Polytechnic Institute and State University, Blacksburg, VA, USA, in 2009, all in electrical engineering. From 1999 to 2004, he was a Senior

Researcher at the Hyosung Heavy Industry R&D Center, Seoul, Korea. In 2009, he was a Postdoctoral Researcher at National Semiconductor Corporation, Santa Clara, CA, USA, involved in a smart home energy management system. In 2016, he was a Visiting Scholar with the Center for Power Electronics Systems (CPES), Virginia Polytechnic Institute and State University, Blacksburg. Since 2010, he has been with Hanyang University, where he is currently an Associate Professor in the Department of Electrical and Biomedical Engineering. His research interests include modeling and control of distirbuted power converter systems, soft-switching techniques, energy management systems in microgrid applications, modular power converter for renewable energies and motor drive systems. Dr. Kim was a recipient of the 2007 First Prize Paper Award from the IEEE IAS.

Jin-Tae Cho He received the B.S. and M.S. degrees in Electrical Engineering from Korea University, Seoul, Korea, in 2006 and 2008, respectively, and he is working toward Ph.D in the area of DC distribution. He is currently a senior researcher at Smart Power Dis-tribution Lab. of KEPRI (Korea Electric Power Corp. Research Institute), Daejeon, Korea. His research interests include protection, monitoring and control of LVDC distribution system.

Seok-Woong Kim He received the B.S. degree in Electrical Engineering from Chungbuk National University and M.S. degree from Hanyang University, Seoul, Korea, in 2012 and 2016, respectively. He is currently a researcher at Basic Research Center for Electric Power of KEPRI (Korea Electric Power Corp. Research Institute), Seoul, Korea. His research interests include Power Conversion System, DC Microgrid, Control algorithm.